Journal of
Ceramic Science
and Technology

J. Ceram. Sci. Tech., **06** [03] 183-190 (2015)
DOI: 10.4416/JCST2014-00051
available online at: http://www.ceramic-science.com

Characterization of Mechanical Properties under Shear Load of a Short-Carbon-Fiber-Reinforced C/SiC Ceramic[1)]

Y. Shi*[1], K. Tushtev[2], D. Koch[1]

[1]Institute of Structures and Design, German Aerospace Center Stuttgart, Germany
[2]Advanced Ceramics, University of Bremen, Germany

received December 5, 2014; received in revised form January 19, 2015; accepted March 10, 2015

Abstract

The main objective of this work is the evaluation of the mechanical shear properties of a short-carbon-fiber-reinforced ceramic, which shows strong non-homogeneity in its microstructure and anisotropy through different fiber orientations. In this work, the shear modulus (G-modulus) and shear strength of this material were determined with the Iosipescu shear test and the Asymmetric-Four-Point-Bend shear test (AFPB test) at room temperature. Both test methods provide a nearly pure shear stress state in the shear plane and are therefore suitable for determination of the mechanical properties under shear load. Different notch opening angles with $\theta = 0°$ or $\theta = 110°$ and sample sizes for both methods are discussed. For strain measurement, strain gauge rosettes are applied on two sides of the test specimens. Because of the limited size of basic material, for the Iosipescu test small specimens were bonded onto aluminum tabs, which induced different failure mechanisms. Therefore the Iosipescu results are only valid for determination of shear modulus but not for evaluation of shear strength.

Keywords: Short-carbon-fiber C/SiC, mechanical properties under shear load, Iosipescu shear test, Asymmetric-Four-Point-Bend shear test, FEM

I. Introduction and Objective

Thanks to their excellent mechanical and thermal properties, carbon-fiber-reinforced silicon carbide (C/SiC) composites have the potential to be used in aerospace technology including in turbines, turbo pumps, nozzles, leading edges, and thermal protection systems. They are also suitable choices for some other applications such as high-performance braking systems [1–5]. While continuous-fiber-reinforced ceramics have been characterized and evaluated in a large number of studies, the use of short-carbon-fiber-reinforced ceramics is in the early stages and only few studies have been published discussing their mechanical properties [6–8].

The determination of material parameters such as density, strength, elastic/shear modulus and others is essential for further application of new composites. Interlaminar shear strength is typically low in long-fiber-reinforced composites and is determined with the short-beam test [9], Iosipescu test [10], AFPB test [11], double-notch method [12], etc. Since short-fiber-reinforced ceramic composites typically have no laminate structure, their shear behavior is dominated by loading and short fiber orientation. Basic requirement of the shear test is the generation of pure and uniform shear stress distribution in the shear plane for accurate determination of shear properties, which is realized in torsion tests of thin tubular samples. For flat composites, a number of test methods have been developed to study both in-plane or interlaminar shear properties. The most commonly used methods for in-plane testing are the Iosipescu test [10, 13], the off-axis tension test [14, 15], the Asymmetric-Four-Point-Bend shear test (AFPB test) [16] and torsion test [17]. For the three-point-bending shear test, the specimen is relatively simple but the shear stress is not uniform through the thickness of the sample. One of the main challenges for the use of the off-axis tension test is the complicated gripping system, which has to ensure accurate loading of the specimen [14, 15]. Although several methods are available to measure both the in-plane and interlaminar shear properties of ceramic composites, there is no well-established method available for short-fiber-reinforced ceramics. On the other hand, fatigue and breakage behavior of short-fiber-reinforced ceramics is complicated. Fig. 1 shows the crack paths of a short-carbon-reinforced structural component (C/SiC with short fiber bundle length of 10 mm and random fiber orientation), which has been damaged as a result of multiple tensile and shear loadings. A clear dependence between the cracks and local fiber bundle orientation can be observed in Fig. 1 and would be compared with the fatigue mechanism of the test sample under shear loading.

This paper discusses the localized shear stiffness and strength of short-carbon-fiber-reinforced ceramic composites. In order to do this, small samples with strong non-homogeneity and limited sample geometry have been extracted from component parts. Based on FEM analysis, the appropriate notch angle for the experiment was determined. The mechanical properties as well as the fracture mechanisms depended on the test methods and the sample sizes were assessed and discussed.

1) All experimental tests and FEM-Analysis in this study were conducted at the Advanced Ceramics, University of Bremen.

* Corresponding author: yuan.shi@dlr.de

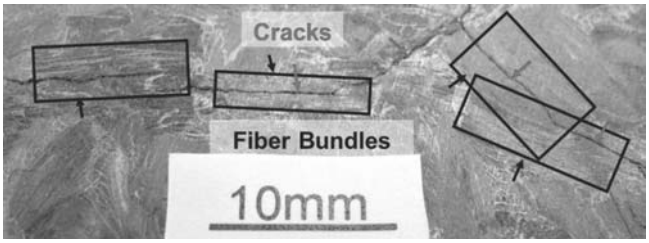

Fig. 1: Crack paths of a damaged short-carbon-fiber-reinforced structural component (C/SiC with short fiber bundle length of 10 mm and random fiber orientation).

II. Experimental

(1) Material description

A short-carbon-fiber-reinforced C/SiC composite with 9 mm fiber length (Long Cut Fiber Composite, LCFC) was tested, which was produced in a three-stage process: hot-pressing, carbonization and liquid silicon infiltration. For microstructural analysis, the non-destructive x-ray imaging technique of Micro-Computed-Tomography (micro-CT) was applied at the University of Bayreuth. A detailed description of the material manufacturing process, the microstructural analysis of the sample and the associated material parameters is given in [18]. The fiber content of the LCFC samples is approx. 45 vol%. The material parameters are summarized in Table 1.

Table 1: Material parameters of the LCFC.

Composite	Fiber volume content [%]	Density [g/cm^3]	Open porosity [%]	Fiber diameter [µm]	Fiber length [mm]
LCFC	45	2.11	3.40	7	9

Fig. 2 shows the polished cross-section of test material with the global coordinate system. With the non-destructive x-ray imaging technique of Micro-Computed-Tomography (micro-CT), the fiber orientation within the specimen could be determined. Analysis of the fiber orientation in the z-direction (perpendicular to the xy-plane in Fig. 2a) was done by analyzing the xz-plane, it was shown that approximately 80 % fibers were located in the xy-plane within an angle of ± 18°. Therefore the orientation of the fiber bundles in z-direction can be negligible [18]. Fig. 2b shows the distribution of the azimuth angle's orientation, which refers to the orientation angle of the short fibers in the xy-plane. It varies between 0° and 180°, whereas 0° or 180° corresponds to the y-direction (perpendicular) and 90° is parallel to the x-direction (longitudinal). In this case, fiber bundles were mainly orientated in x-direction (90° ± 20°). In contrast to monolithic ceramics or many continuous fiber-reinforced ceramics, a considerable inhomogeneity resulting from the fiber orientation and the relatively long fiber length can be clearly observed in Fig. 2.

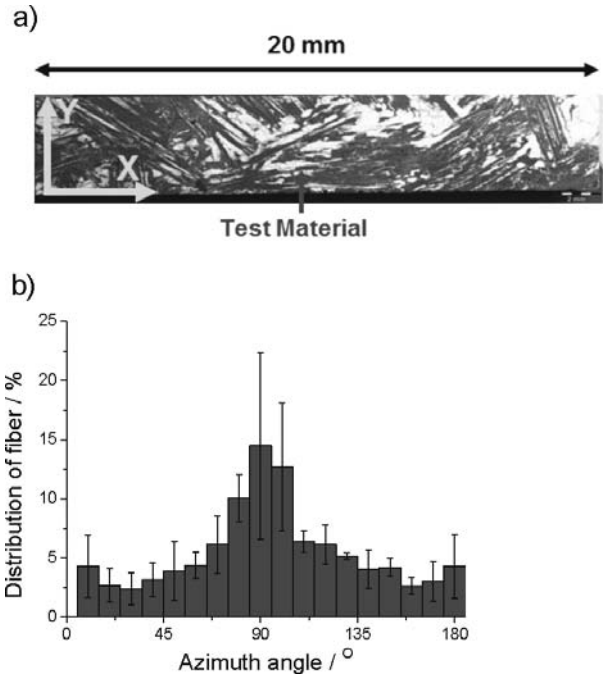

Fig. 2: a) Polished cross-section of test material with the global coordinate system; gray: carbon fiber bundles, white: matrix; b) Distribution of fiber orientation in the xy-plane [18].

(2) Sample preparation and test methods

For Iosipescu shear tests, normally samples with the the dimensions of 80^L x 20^W x 10^H mm^3 [19] are prepared by means of sawing and polishing with a diamond saw and diamond suspension. The manufacturing of such large Iosipescu samples was not possible for LCFC because of the limited size as the specimens were cut out of component parts. Therefore small C/SiC samples with dimensions 5^L x 16^W x 11^H mm^3 were bonded onto aluminum tabs (see Fig. 3a) with a centrally positioned U-shaped channel, and then the samples were notched on both sides. In contrast to the Iosipescu test, the use of samples (40^L x 8^W x 5^H mm^3 [20]) without tabs makes the AFPB test very attractive (AFPB C/SiC sample in Fig. 3b). All samples were prepared with fiber bundles mainly orientated in the x-axis (Fig. 2 and Fig. 3).

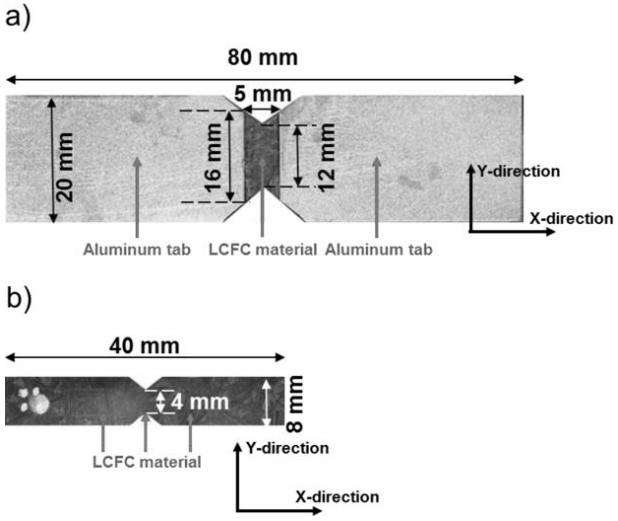

Fig. 3: a) Iosipescu sample (Dimensions 5 x 16/12 x 10 mm^3) with aluminum tabs (dimensions 80 x 20 x 10 mm^3); b) AFPB sample (dimensions 40 x 8/4 x 5 mm^3).

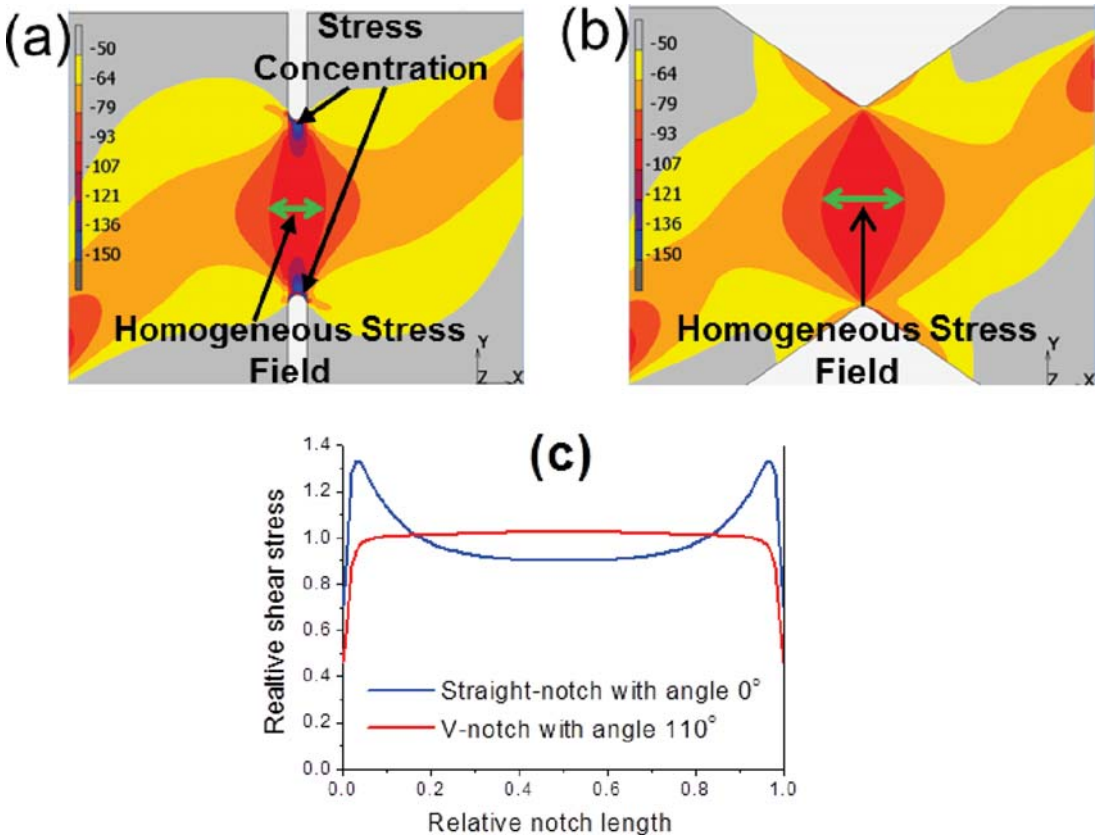

Fig. 4: Influence of the notch angle on the shear stress distribution and concentration, a) Straight-notched with the notch angle $\theta = 0°$, b) V-notched with the notch angle $\theta = 110°$, c) normalized shear stress-notch length diagram.

To induce a homogenous stress field in the loading zone, the samples for both methods, Iosipescu and AFPB, were notched to approx. 25 % depth of the sample's width [19, 20]. While the dependence of the notch angle and material anisotropy or fiber orientation on mechanical properties for continuous-fiber-reinforced composite material has been discussed in [21, 22], no publication was found discussing the relevance for short-fiber composites. In order to determine the effect of different notch angles on the stress distribution and stress concentration between notches, linear-elastic finite-element-method (FEM) simulation was applied using MSC Marc 2010 with Intel ® Visual Fortran Compiler with eight-node quadrilateral elements (Fig. 4). The elastic constants of the LCFC were determined by means of pretests under tension, compression in the x- and y-direction and shear load in the xy-plane [8]. The material showed a different Young's Modulus under tension and compression load. The material constants shown in Table 2 were used for the FEM simulation in a 2D model with coordinate system in the x- and y-direction.

The distribution of shear stress in the loading direction is shown in Fig. 4a and b with same color scale. The stress concentration surrounding the straight notch in Fig. 4a is locally higher compared to the V-notch in Fig. 4b. With the angle of 110°, the width of the homogeneous shear stress field expands (green double arrows in Fig. 4a and b), which is very important for reliable strain measurement using strain gauges. Furthermore, the shear stress curve of the V-notch is much more homogeneous than straight-notch (Fig. 4c). Therefore, samples for both the Iosipescu and AFPB tests were notched with the same angle of 110°.

Table 2: Material properties of the LCFC for the FEM elastic calculations.

	Young's Modulus E (Tension) [GPa]	Young's Modulus E (Compression) [GPa]	G-Modulus G [GPa]	Poisson's ratio
x-Direction	94	85	G_{12}=21	ν_{21}=0.10
y-Direction	60	66		

Fig. 5a shows the Iosipescu test fixture. The prepared specimens were aligned in the test configuration with help of the alignment device which can be moved into the notch of the sample.

For the Iosipescu test, shear stress $\tau_{losipescu}$ within the notched cross section is:

$$\tau_{losipescu} = \frac{P}{wt} \quad (1)$$

where P is the applied load, w is the average specimen height between the notches and t is the thickness of the sample (here $w = 12\ mm$ and $t = 10\ mm$ (Fig. 3a)).

The AFPB test fixture had an outer and an inner span with distances $L_o = 36\ mm$ and $L_i = 12\ mm$ (Fig. 5b). In contrast to the Iosipescu test, the shear stress generated in the AFPB test depends on the fixture dimensions:

$$\tau_{AFPB} = \frac{P(L_0 - Li)}{wt(L0 + Li)} \quad (2)$$

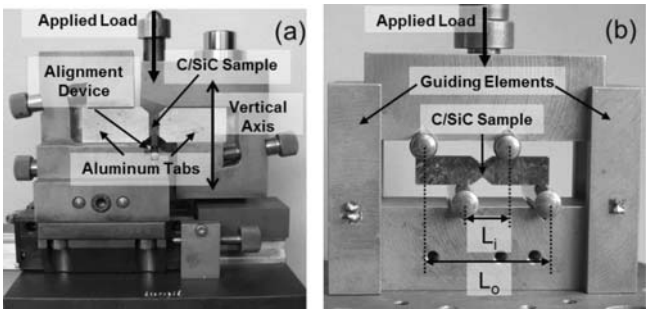

Fig. 5: Test fixtures used in this study: a) Iosipescu fixture with vertical axis for easy movement and alignment device; b) AFPB test fixture with outer and inner span distances of L_o = 36 mm and L_i = 12 mm, the rollers for load introduction had a diameter of 8 mm

The shear modulus *G* was determined from the initial linear range of shear stress-strain curves. For strain measurement, two strain gauge rosettes were applied on both sides in ±45° to the applied loading direction. One important reason for the measurement on front and back sides is that undesired specimen deformation, e.g. twisting, can be registered if it occurs. The shear strain γ was derived from the measured strains ε_{+45} (at an angle of + 45° to the longitudinal axis) and ε_{-45} (at an angle of - 45° to the longitudinal axis) of the strain gauge rosettes:

$$\gamma = \varepsilon_{+45} - \varepsilon_{-45} \quad (3)$$

With the resulting stress-strain diagram the shear module can be calculated in the linear-elastic range:

$$G = \frac{\tau}{\gamma} \quad (4)$$

All shear tests were performed up to failure with a universal testing machine (Zwick 005) in displacement control with a cross-head speed of 1 mm/min. For statistical reasons, three to five samples were tested.

III. Results and Discussion

The fracture paths of the failed specimens as a result of the Iosipescu and AFPB tests are shown in Fig. 6a and c. For a detailed presentation of the fracture path, selected samples were also examined with a scanning electron microscope (SEM) (Fig. 6b and d). Different failure mechanisms between both methods are clearly recognized in Fig. 6a and c. The fractured path of the Iosipescu sample is almost parallel to the shear force direction and the bonding surface between the LCFC material and aluminum tabs. Along the shear plane, which is the weakest part of the whole test sample, there is no fiber bridging but only matrix, fiber-matrix-interface or existing pores. The failure mechanism is macroscopic shear. It should be noted that, based on the analysis of SEM micrograph in Fig. 6b, the fracture path does not lie in the hardened adhesive boundary layer.

Compared to the Iosipescu test, a different failure mechanism is observed in the AFPB samples (Fig. 6c), where multiple cracks occurred along fiber bundles. Since most of the short fibers are oriented in the longitudinal x-direction (in Section (1), the existing and new emerging cracks spread mainly along matrix area, interfaces between fiber and matrix or within fiber bundles, which represent weak areas of LCFC.

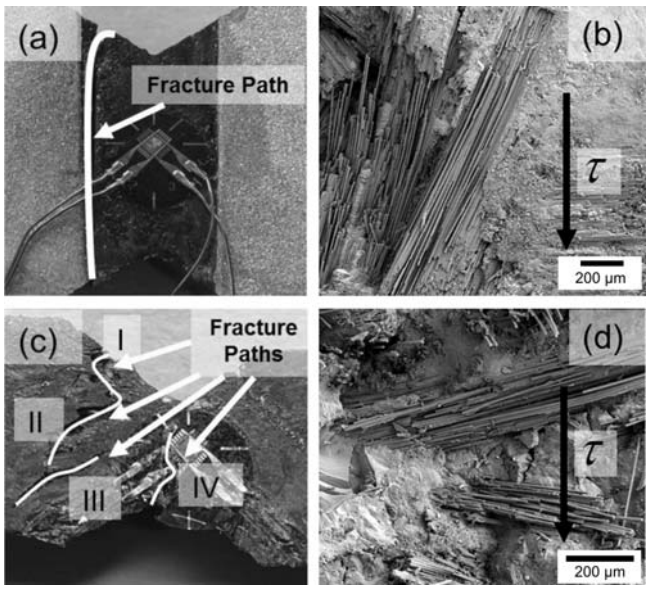

Fig. 6: Sheared samples after the Iosipescu and AFPB tests: a) Fracture path of the Iosipescu sample; b) SEM micrograph of the fracture path of the Iosipescu sample; c) Fracture paths of the AFPB sample from I to IV; d) SEM micrograph of the fracture path of the AFPB sample

From the SEM micrograph of the fracture path for test samples in Fig. 6b and d, no single fiber pull-out effect can be observed. This means that the cracks always propagate along the weak areas to spread further and show high dependence on fiber orientation. The inhomogeneity of the investigated LCFC causes a complicated macroscopic multiple cracking, which ultimately leads to a final failure of the AFPB samples.

In order to understand the shear failure mechanisms in detail, linear-elastic FEM simulation was performed with the same settings and material parameters as mentioned in Section (2). Fig. 7a shows the Von Mises equivalent stress distribution of V-notch with 110°. In addition to the peak value in the area between notches, another two peak values, which are in the same stress level, occur near the notch edges. The possible reason lies in the superimposed bending moment in this area. Fig. 7b and c show the normal-stress in x- and y-direction with the peak values. These stress concentration areas, the short fiber orientation and the weak spots in the material lead together effectively to the macroscopic multiple cracking, which was in agreement with the real fracture paths of the AFPB sample shown in Fig. 6c. The fracture path from I to III is attributed to the stress concentrations near the notch edges and the area between notches leads to final fracture at path IV. The stress state within the microstructure results from the strong inhomogeneity and is therefore very complex: tension, compression and bending stresses are induced during loading.

Fig. 8 shows the schematic representations of the fiber bundles orientation and crack paths for both tests. In the

case of the Iosipescu sample, the fractured path changed the direction and spread further along the weak spots.

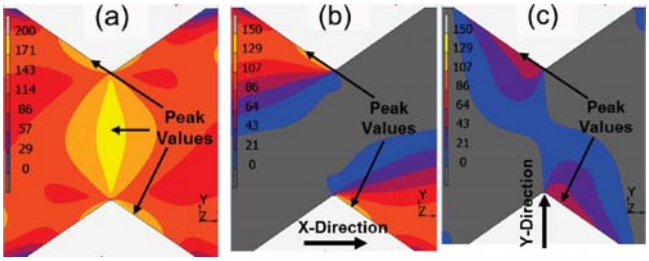

Fig. 7: Stress distribution of V-notch with angle 110°: a) Von Mises equivalent stress with color scale 0 to 200 MPa; b) Normal stress in x-direction with color scale 0 to 150 MPa; and c) Normal stress in y-direction with color scale 0 to 150 MPa.

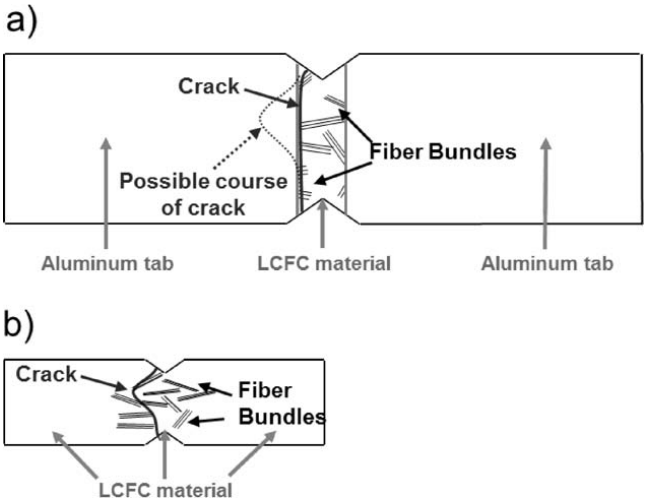

Fig. 8: Schematic representation of the short fiber bundles orientation and crack paths of a shear sample within the notch area: a) Iosipescu sample with aluminum tabs, the dotted line shows possible course of the crack; b) AFPB sample.

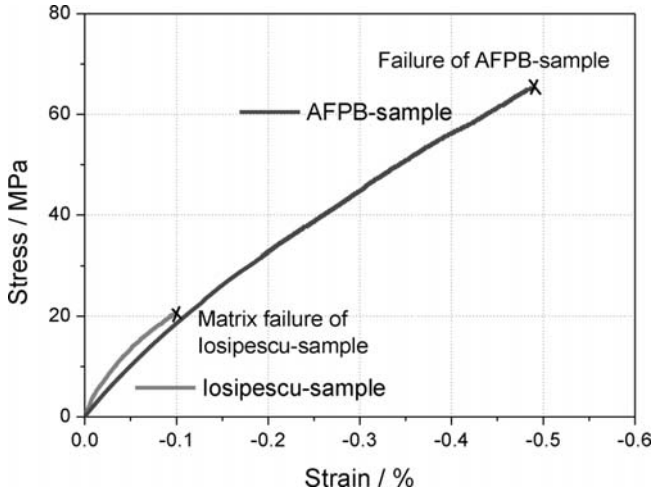

Fig. 9: Typical shear stress-strain curves of the Iosipescu and AFPB samples.

Typical shear stress-strain curves out of three to five results obtained from LCFC specimens by both shear tests are shown in Fig. 9. The AFPB test shows an initial elastic behavior below stresses of approx. 10 MPa, followed by nonlinear behavior with continuously decreasing shear modulus. Also shown in Fig. 9 is the curve of tested Iosipescu sample with similar initial elastic behavior below approx. 10 MPa. Compared to the AFPB samples, the observed shear strength and reached strain to failure of Iosipescu samples are significantly smaller.

The measured values including standard deviation for Iosipescu and AFPB samples are shown graphically in Fig. 10. The difference of the average shear strength for both test methods is clearly marked in Fig. 10a. However, the shear modulus is not largely influenced by almost same standard deviation for both test methods (Fig. 10b).

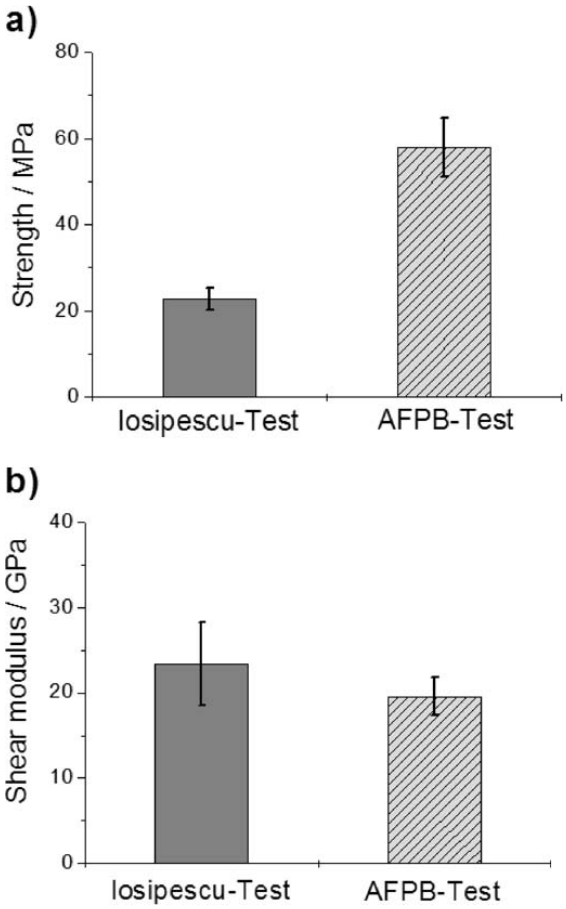

Fig. 10: a) Shear strength and b) shear modulus with standard deviation of the material LCFC determined in the Iosipescu test and the AFPB test.

Owing to the different failure mechanisms observed in Fig. 6, Iosipescu samples with the macroscopic shear failure showed clearly lower shear strength and relative smaller standard deviation than AFPB samples. The shear yield strength values (approx. 10 MPa) were found to be similar for both test methods (Fig. 9) and the determined elastic shear moduli are almost same (Fig. 10b). However, beyond the proportional limit, the two tests present different results (Fig. 10a), which is attributed to the different failure mechanisms (Fig. 6). We can assume that the results from the measurement for shear strength with the two

methods should be similar by approx. 60 MPa (Fig. 10a), if the Iosipescu tests could be performed with large samples and without aluminum tabs. However, owing to the limited size of given material, the manufacturing of such large Iosipescu samples was not possible for LCFC material.

According to the DIN EN 12289 for the determination of the in-plane shear properties of advanced technical ceramics, the test results presented in this work would not be considered to be valid because of the type of rupture. Considering the fracture path of the short-fiber-reinforced structure component (C/SiC) shown in Fig. 1, it cannot be expected that an ideal fracture path will emerge in the predefined area between the notches for both test methods. The cracks and fracture paths show an obvious dependence on local fiber orientation and may always spread across the matrix area, the interface between fiber and matrix or within the fiber bundle. Therefore, not only the shear modulus through both methods indicated in Fig. 10b but also the determined shear strength using the AFPB method with the whole shear sample (approx. 60 MPa) could be reliably documented as the characteristic values of the investigated non-homogenized short-carbon-fiber-reinforced ceramic.

IV. Conclusions

For the characterization of the shear properties of a short-carbon-fiber-reinforced ceramic with strong non-homogeneity, two different test methods, the Iosipescu and AFPB methods, both providing a nearly pure shear stress state at the shear plane, were applied at room temperature. Based on the FEM calculations of stress analysis, an acceptable stress concentration around the V-notch could be achieved with an angle of 110° and the width of the homogeneous stress field in the shear range has been expanded. Therefore, the samples for both the Iosipescu and AFPB tests were notched with same angle.

Because of the limited size of basic material, the manufacturing of a complete Iosipescu sample from LCFC was not possible. Instead, an alternative method was applied using small samples that are bonded onto aluminum tabs and then notched on both sides, which leads to different failure mechanisms of the two methods. Without fiber bridging but only matrix, fiber-matrix-interface or existing pores and cracks, the area parallel to the shear force and the bonding surface between LCFC material and aluminum tabs become the weakest part of the whole Iosipescu test sample. In contrast to these results, local failure owing to multiple macro-cracking has been observed in AFPB samples, which is induced by the interaction between fiber orientation and loading direction. The cracks always propagate along the weak areas to spread further and show high dependence on fiber orientation. On the other hand, the varying local fiber orientation of the investigated material leads to macroscopic multiple cracking, and final shear failure of the samples. The results of stress distribution with peak values from numerical simulation showed agreement with the real fracture paths of the AFPB sample.

Both the Iosipescu and AFPB test methods provided a good possibility for the determination of the shear modulus. The shear yield stresses and G-modulus were found to be similar for the LCFC material, which implies that there is no significant difference between the two methods for the measurement of shear property in initial elastic areas. The determined shear strength using the AFPB method with complete sample could be reliably documented as the characteristic values of the investigated composite material because of the conformed fracture mechanism compared with the damaged structure component.

References

1 Herbell, T.P., Eckel A.J.: Ceramic matrix composites for rocket engine turbine applications, *J. Eng. Gas. Turb. Power,* **115**, [1], 64 – 69, (1993).

2 Christin, F.: Design, fabrication, and application of thermostructural composites (TSC) like C/C, C/SiC, and SiC/SiC composites, *Adv. Eng. Mater*., **4**, [12], 903 – 912, (2002).

3 Naslain, R.R.: SiC-matrix Composites: nonbrittle ceramics for thermo-structural application, *Int. J. Appl. Ceram. Tec.*, **2**, 75 – 84, (2005).

4 Zhang, Y., Xu, Y., Lou, J., Zhang, L., Cheng, L., Lou, J., Chen, Z.: Braking behavior of C/SiC composites prepared by chemical vapor infiltration, *Int. J. Appl. Ceram. Tec*., **2**, 114 – 121, (2005).

5 Krenkel, W., Renz. R.: Ceramic matrix composites: fiber reinforced ceramics and their applications, 2008, WILEY-VCH, Weinheim.

6 Yang, F.Y., Zhang, X.H., Han, J.C., Du, S.Y.: Mechanical properties of short carbon fiber reinforced ZrB2-SiC ceramic matrix composites, *Mater. Lett.*, **62**, [17 – 18], 2925 – 2927, (2008).

7 Thielicke, B., Neubrand, A., Kienzle, A.: Four point bending tests of a C/SiC material for industrial application under quasistatic and cyclic loading, 5th International Conference on High-Temperature Ceramic Matrix Composites – HTCMC5, 205 – 210, (2004).

8 Shi, Y., Tushtev, K., Koch, D., Rezwan, K.: Mechanical characterization and non-linear modelling of anisotropic, Short-Fibre-Reinforced Ceramics, (in German), 18. Symposium Verbundwerkstoffe und Werkstoffverbunde, Chemnitz, 178 – 183, (2011).

9 Kedward, K.T.: On the short beam test method, *Fibre Sci. Technol.*, **5**, [2], 85 – 95, (1972).

10 Broughton, W.R., Kumosa, M., Hull, D.: Analysis of the iosipescu shear test as applied to unidirectional carbon-fibre reinforced composites, *Compos. Sci. Technol.*, **38**, [4], 299 – 325, (1990).

11 Ünal, Ö., Dayal, V.: Interlaminar shear strength measurement of ceramic composites by asymmetric four point bend shear test, *Mater. Sci. Eng. A*., **340**, [1 – 2], 170 – 174, (2003).

12 Dadras, P., McDowell, J.S.: Analytical and experimental evaluation of double-notch shear specimens of orthotropic materials, *Exp. Mech.*, **30**, 184 – 189, (1990).

13 Iosipescu, N.: New accurate procedure for single shear testing of metals, *J. Mater.*, **2**, 537 – 566, (1967).

14 Marín, J.C., Cañas, J., París, F., Morton, J.: Determination of G12 by means of the off-axis tension test. Part I: Review of gripping systems and correction factors, *Compos. Part A Appl. S.,* **33**, [1], 87 – 100, (2002).

15 Marín, J.C., Cañas, J., París, F., Morton, J.: Determination of G12 by means of the off-axis tension test. Part II: A self-consistent approach to the application of correction factors, *Compos. Part A Appl. S.,* **33**, [1], 101 – 111, (2002).

16 Ünal, Ö, Anderson, I.E., Maghsoodi, S.I.: A test method to measure shear strength of ceramic joints at high temperatures, *J. Am. Ceram. Soc.*, **80**, [5], 1281 – 1284, (1997).

[17] Foley, G.A., Roylance, M.E., Houghton, W.W.: Use of torsion tubes to measure in-plane shear properties of filament wound composites, *Am. Soc. Test. Mater.*, 208, (1989).

[18] Shi, Y., Tushtev, K., Hausherr, J., Koch, D., Rezwan, K.: Oxidation kinetics and its impact on the strength of carbon short fiber reinforced C/SiC ceramics, *Adv. Eng. Mater.*, **15**, [1 – 2], 19 – 26, (2013).

[19] DIN EN 12289 Advanced technical ceramics – Mechanical properties of ceramic composites at ambient temperature – Determination of in-plane shear properties, 2005.

[20] ASTM-C1469 – 00-Standard Test Method for Shear Strength of Joints of Advanced Ceramics at Ambient Temperature, 2000.

[21] Adams, D.F.: The iosipescu shear test method as used for testing polymers and composite materials, *Polym. Composite*, **11**, [5], 286 – 290, (1990).

[22] Melin, L.N., Neumeister, J.M.: Measuring constitutive shear behaviour of orthotropic composites and evaluation of the modified iosipescu test, *Compos. Struct.*, **76**, 106 – 115, (2006).